Robotica (2007) volume 25, pp. 147–156. © 2007 Cambridge University Press
doi:10.1017/S0263574706003328 Printed in the United Kingdom

Dynamic redundancy resolution in a nonholonomic wheeled mobile manipulator

Glenn D. White, Rajankumar M. Bhatt and Venkat N. Krovi*

Department of Mechanical and Aerospace Engineering, State University of New York at Buffalo, Buffalo, NY 14260, USA
E-mails: gdwhite@eng.buffalo.edu, rmbhatt@eng.buffalo.edu

(Received in Final Form: December 22, 2006)

SUMMARY
Wheeled Mobile Manipulators (WMM) possess many advantages over fixed-base counterparts in terms of improved workspace, mobility and robustness. However, the combination of the nonholonomic constraints with the inherent redundancy limits effective exploitation of end-effector payload manipulation capabilities. The dynamic-level redundancy-resolution scheme presented in this paper decomposes the system dynamics into decoupled task-space (end-effector motions/forces) and a dynamically consistent null-space (internal motions/forces) component. This simplifies the subsequent development of a prioritized task-space control (of end-effector interactions) and a decoupled but secondary null-space control (of internal motions) in a hierarchical WMM controller. Various aspects of the ensuing novel capabilities are illustrated using a series of simulation results.

KEYWORDS: Decoupled task- and null-space dynamic control; Dynamic redundancy resolution; Nonholonomic mobile manipulator.

1. Introduction

Partially- or fully-autonomous robotic systems have proven very useful in extending the reach of humans in numerous manipulation and environment interaction tasks. Over several decades, the fixed-base serial-chain configuration has been the mainstay of robotic manipulation systems. However, increasingly complex manipulatory tasks can be performed by mounting such robotic manipulators on a mobile base, creating the so-called *mobile manipulator* configuration. The resulting mobile manipulators have been deployed in numerous application arenas—ranging from gantry-mounted manipulators on the shop floor to highway maintenance robots to robotic earth-moving excavators to free-flying satellite-repair robots.

In this paper, we will focus attention on various aspects of manipulation of end-effector payloads by a prototypical Wheeled Mobile Manipulator (WMM) system, consisting of a differentially driven Wheeled Mobile Robot (WMR) base with a mounted planar two-link two revolute-joint manipulator arm. Our ultimate application arena is for cooperative payload transport as shown in Fig. 1, where a group of such WMM modules come together for payload transport. To this end, it is critical to develop a semi-autonomous decentralized control framework wherein each WMM module is able to independently control its own end-effector interactions (motions/forces) with respect to the payload. The entailed issues and challenges, discussed briefly below, serve to focus our research efforts.

The manifestation of redundancy, at both the kinematic and actuation levels, is a prominent feature of mobile manipulators. Such redundancy, also seen in the WMM configuration, bestows many advantages including flexibility and robustness to disturbances. WMM systems now possess considerable flexibility in producing desired motion/force at the end-effector (using only the base, only the manipulator-arm, or by some combination of the two). Redundancy also confers the ability to mechanically accommodate, detect, and compensate for motion/force disturbances within the articulated structure.

However, both the design selection and subsequent control needs to be done carefully in order to realize these benefits. From a *design perspective*, the selection process needs to be performed to satisfy performance criteria. For example, selection of the topology (type and number of articulations) dimensions (link-lengths/offsets/mass-distribution), actuation (type and location of actuators) of individual WMM modules is of vital importance. However, these challenges are assumed to have been addressed elsewhere[1,2] resulting in selection of a kinematically redundant fully-actuated nonholonomic WMM. From a *control perspective*, a suitable resolution of such redundancy is required to achieve the performance benefits. The determination of the actuator rates/forces, for a given end-effector motion of a redundant manipulator, is typically an underconstrained problem but essential for planning/control of such systems. Numerous kinematic and dynamic redundancy resolution methods are available in the literature (and will be briefly reviewed). However, none of these can be directly applied for dynamic redundancy resolution in nonholonomic WMMs—the development of such a strategy is the principal research goal of this paper. Further, we discuss the feasibility of decoupling of the dynamics into task-space and null-space components and prioritized satisfaction of the task-space goals.

The rest of this paper is organized as follows: In Section 2, we briefly review the pertinent literature on redundancy resolution at the kinematic and dynamic levels with a focus on mobile manipulator systems. The dynamic equations of motion for the WMM are developed in Section 3 for use

*Corresponding author. E-mail: vkrovi@eng.buffalo.edu

https://doi.org/10.1017/S0263574706003328 Published online by Cambridge University Press

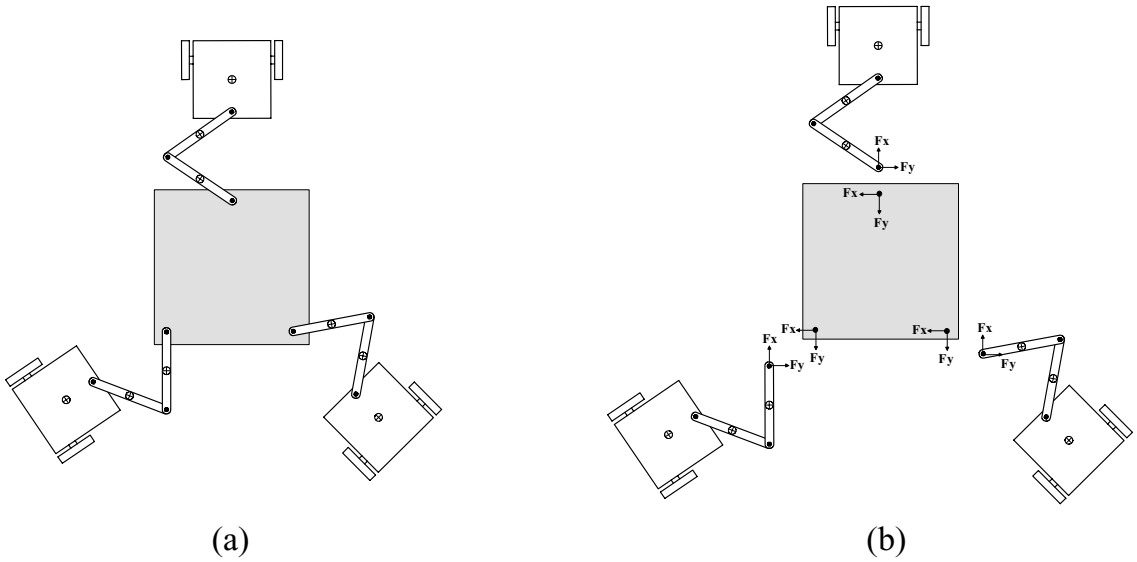


Fig. 1. Robot collective. (a) Three robots interacting with a common payload. (b) Robots decoupled from payload.

in subsequent analysis. Section 4 presents various aspects of development of a dynamic redundancy resolution method that allows for independent control of both the task-space (end-effector) and the null-space (mobile base) outputs. Simulation results are used to illustrate various facets of the simultaneous task- and null-space control in Section 5. Section 6 concludes with a discussion of the results.

2. Background

Mobile manipulator systems are typically composed of a mobile base with one (or more) mounted manipulators.[3–6] While track-, gantry- or manipulator-bases may be modeled and analyzed easily, WMR bases offer special challenges. WMRs cannot be stabilized to a single equilibrium point by a continuous (smooth) time-invariant pure state feedback law, due to the violation of Brockett's condition.[7] Hence, the motion planning and control of such WMRs requires special treatment.[8–11] Concomitantly, the class of nonholonomic WMM with such bases requires careful handing.

Further, combining the mobility of the base platform and the mounted manipulator creates both kinematic and actuator redundancy.[3–6] The determination of the actuator rates/forces for a given end-effector motions/forces in a redundant manipulator is typically an underconstrained problem (but essential for motion planning/control). See Nakamura[12] for a review of these methods.

At the kinematic level, the combined system typically possesses more internal degree-of-freedom (DOF) than necessary to perform the task. Most of the redundancy resolution methods in the literature have a principal underlying theme of optimizing a measure of performance based on the kinematics of the system. Several of these results have been extended and applied to WMMs. For example, Seraji[3] extended Whitney's[13] approach to kinematic redundancy resolution of mobile manipulators. Alternatively, Yamamoto and Yun[5] decompose the motions of the mobile manipulator into decoupled WMR-base and manipulator subsystems. The WMR is then controlled so as to bring the manipulator to a preferred configuration (using criteria such as the manipulability measure) as the end-effector performs a variety of unknown manipulation tasks. In contrast, Colbaugh *et al.*[6] exploit the kinematic redundancy in nonholonomic systems to simplify the control by creating a reduced dynamic model (in terms of independent configuration variables) together with the purely kinematic relationship (coupling the independent configuration variables to the extended configuration variables). However, in all above cases, the focus is on kinematic-level redundancy resolution and implicitly assumes the availability of good rate-control actuators.

Far lesser literature discusses actuator-redundancy resolution within the redundant system. In exactly actuated systems, only as many components of the motions/forces as degrees of actuation can be controlled. However, in redundant systems, it is meaningful to exploit the surplus actuator inputs to achieve secondary goals, in addition to primary task performance. Traditionally, such secondary criteria have included either the contact- or internal-force distribution—this giving rise to the various hybrid position/force control schemes frequently seen in multilegged walkers,[14] multifingered hands,[15] and multiarm systems.[16]

An alternate partitioning into a primary (end-effector) and secondary (internal-motion) spaces is also possible. Khatib[17] proposed a method of controlling redundant serial-chain systems by projecting the system dynamics into the operational space to realize an end-effector dynamic model together with a dynamically consistent actuation that provides decoupled control of joint motions in the null-space. This was subsequently extended for mobile manipulator systems with holonomic bases and fully actuated manipulators.[18] Similarly Tan *et al.*[19] controlled a similar holonomic mobile manipulator to manipulate a passive nonholonomic cart along straight lines, corners, or sinusoidal trajectories. However, nonholonomic constraints introduced by the WMR bases limit the capabilities for exerting/resisting arbitrary motions/forces in task space. The effective control of end-effector motion/force outputs is a critical precursor

https://doi.org/10.1017/S0263574706003328 Published online by Cambridge University Press

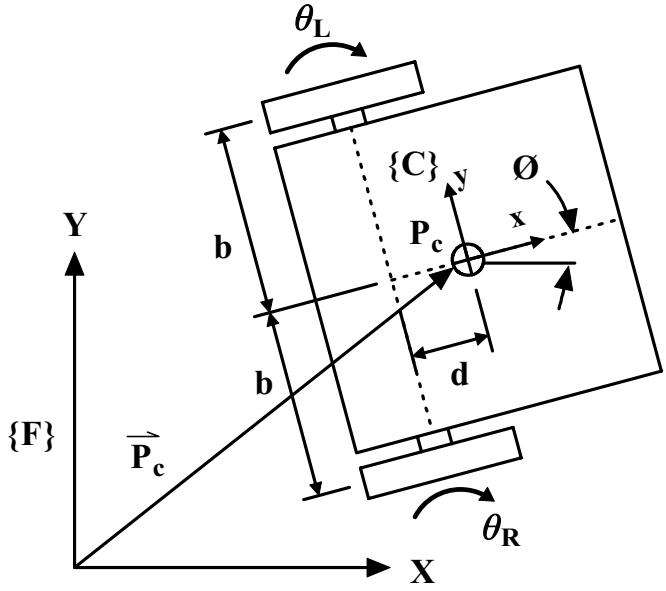


Fig. 2. Wheeled mobile base and kinematic nomenclature.

to decentralized payload manipulation operations by the nonholonomic WMMs and will serve to focus our work.

3. Nonholonomic Mobile Manipulator Modeling

3.1. Kinematic modeling

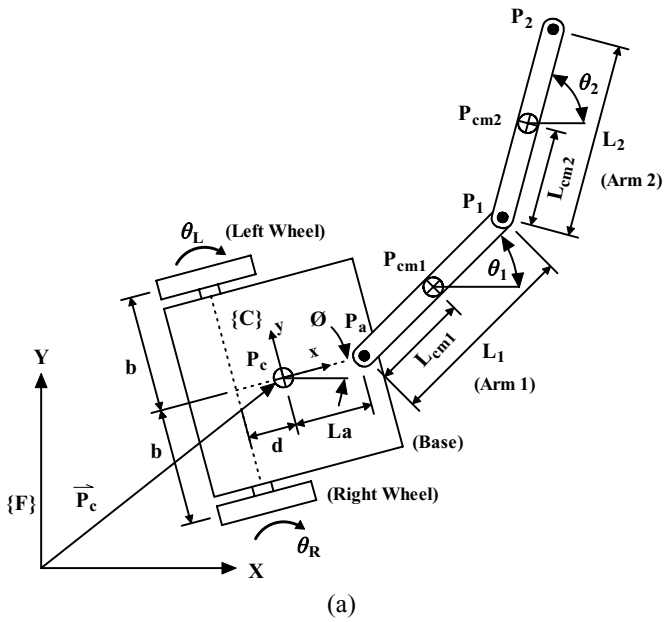
The creation of a kinematic model (together with other pertinent kinematic relationships/constraints) is a vital precursor to any subsequent dynamic analysis. We largely follow the notation of Sarkar *et al.*[20] developed in the context of a WMR and extend it for the WMM case.

A body fixed frame $\{C\}$, attached at the center of mass of the WMR determines the pose with respect to the fixed ground frame $\{F\}$, as shown in Fig. 2. The mobile base is actuated by two independently driven wheels located at an equal distance b on either side of the midline. The drive-wheel axes are collinear and are located at a perpendicular distance $d \geq 0\,\text{m}$ from the center of mass. A passive MECANUM-type omnidirectional nose-wheel provides stable-support to the mobile base (without adding further constraints) and will not be factored in the mathematical modeling.

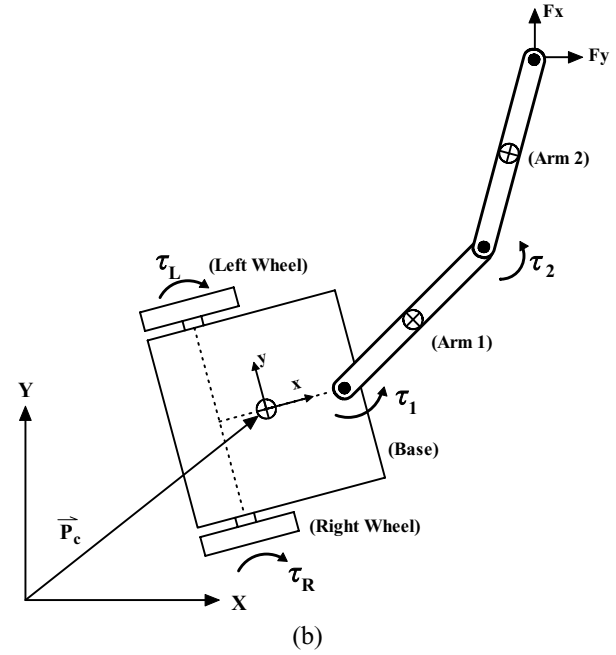
The instantaneous WMR base configuration can be fully described by the following extended set of $k(=5)$ generalized coordinates $\underline{q}_b = [x_c \;\; y_c \;\; \phi \;\; \theta_R \;\; \theta_L]^{\mathrm{T}}$, subject to $m(=3)$ constraints. The first constraint accounts for the nonholonomic behavior of the wheels and restricts the velocity of the WMR in the lateral directions to be zero.

$$-\dot{x}_c \sin\phi + \dot{y}_c \cos\phi - \dot{\phi} d = 0. \tag{1}$$

The other two constraints, relating the base velocities $\dot{x}_c, \dot{y}_c, \dot{\phi}$ and the wheel velocities $\dot{\theta}_R, \dot{\theta}_L$, ensure the no-slip condition at each rolling wheel in the forward directions.



(a)



(b)

Fig. 3. WMM nomeclature. (a) Kinematic parameters. (b) Dynamic parameters.

$$\dot{x}_c \cos\phi + \dot{y}_c \sin\phi + b\dot{\phi} = r\dot{\theta}_R \tag{2}$$

$$\dot{x}_c \cos\phi + \dot{y}_c \sin\phi - b\dot{\phi} = r\dot{\theta}_L. \tag{3}$$

As shown in Fig. 3, the WMM is created by attaching a two-link, two-revolute-joint linkage to the mobile base at the point P_a. The manipulator is assumed to be fully actuated and operates solely in the horizontal plane. Tables 1 and 2 in Appendix B show the various kinematic and dynamic parameters as well as the nomenclature associated with the WMM modeling.

The full set of extended generalized coordinates (of size $N \times 1$), including the manipulator configuration variables, can be described as $\underline{q} = [x_c \; y_c \; \phi \; \theta_R \; \theta_L \; \theta_1 \; \theta_2]^{\mathrm{T}}$. The forward position and velocity kinematics equations (at various points of interest $\{C\}$, $\{CM1\}$, $\{CM2\}$, $\{2\}$) are created in terms of

https://doi.org/10.1017/S0263574706003328 Published online by Cambridge University Press

this extended configuration–variable set for use in subsequent dynamic analyses. The m constraints can be written as

$$A(\underline{q})\dot{\underline{q}} = 0 \tag{4}$$

where

$$A_{m\times N} = \begin{bmatrix} -\sin\phi & \cos\phi & -d & 0 & 0 & 0 & 0 \\ -\cos\phi & -\sin\phi & -b & r & 0 & 0 & 0 \\ -\cos\phi & -\sin\phi & b & 0 & r & 0 & 0 \end{bmatrix}.$$

We can now find an appropriate null-space matrix S that satisfies $AS = 0$. The set of feasible velocities may be expressed in terms of a suitable vector of $n = N - m$ independent velocities, $\dot{\underline{z}}_{n\times 1} = [\dot{\theta}_R \;\; \dot{\theta}_L \;\; \dot{\theta}_1 \;\; \dot{\theta}_2]^{\mathrm{T}}$ as

$$\dot{\underline{q}}_{N\times 1} = S\dot{\underline{z}}_{n\times 1} \tag{5}$$

where $c = r/2b$ and

$$S_{N\times n} = \begin{bmatrix} c(b\cos\phi - d\sin\phi) & c(b\cos\phi + d\sin\phi) & 0 & 0 \\ c(b\sin\phi + d\cos\phi) & c(b\sin\phi - d\cos\phi) & 0 & 0 \\ c & -c & 0 & 0 \\ 1 & 0 & 0 & 0 \\ 0 & 1 & 0 & 0 \\ 0 & 0 & 1 & 0 \\ 0 & 0 & 0 & 1 \end{bmatrix}.$$

We consider the task-space to consist solely of the xy-position of the end-effector. Hence, for subsequent analysis, we also determine the Jacobian that relates the extended joint rates $\dot{\underline{q}}$, to the task-space velocity $\dot{\underline{x}}$, as

$$\dot{\underline{x}}_{p\times 1} = \left[J_q\right]\dot{\underline{q}}_{N\times 1} \tag{6}$$

where

$$[J_q]_{p\times N} = \begin{bmatrix} 1 & 0 & -L_a\sin\phi & 0 & 0 & -L_1\sin\theta_1 & -L_2\sin\theta_2 \\ 0 & 1 & L_a\cos\phi & 0 & 0 & L_1\cos\theta_1 & L_2\cos\theta_2 \end{bmatrix}.$$

Finally, by substituting the relationship $\dot{\underline{q}} = S\dot{\underline{z}}$ into Eq. (6) we get the transformed Jacobian $[J]_{p\times n}$ relating the task space to the independent joint rates as

$$\dot{\underline{x}}_{p\times 1} = [J_q S]\dot{\underline{z}} = [J]\dot{\underline{z}}_{n\times 1}. \tag{7}$$

3.2. Dynamic modeling

We employ a Lagrangian formulation to develop the governing equations of motion (EOM) for the WMM. The WMM is considered to be composed of five distinct rigid bodies—right wheel, left wheel, mobile base, manipulator link 1, and manipulator link 2—with known mass and inertial properties. We consider ideal linear damping to exist at the two wheels and the two manipulator revolute joints. Actuator torque in the system is considered to be produced from "ideal" torque-controlled motors located at each joint. Damping within the motors is considered to be lumped into the idealized damping at each of the four joints. The end-effector is assumed to attach to the environment through a pin-joint connection. Thus, all. end-effector/environment interaction forces are pure forces (with x-y components) and no moment is transmitted. The nomenclature and numerical values for various dynamic parameters are shown in Table 2 in Appendix B. The dynamic EOM for the WMM system may be written as

$$\begin{gathered} H_u(\underline{q})\ddot{\underline{q}} + \underline{V}(\underline{q}, \dot{\underline{q}}) = E\underline{\tau}_m + E_2\underline{F} - A^T\underline{\lambda} \\ A\dot{\underline{q}} = 0 \end{gathered} \tag{8}$$

where H_u is the $N \times N$ inertia matrix expressed in terms of the extended coordinate set, $V(\underline{q}, \dot{\underline{q}})$ includes Coriolis, centrifugal and gravity forces, $\underline{\tau}_m = [\,\tau_R \;\; \tau_L \;\; \tau_1 \;\; \tau_2\,]^{\mathrm{T}}$ consists of the two wheel and two arm motor inputs, and $\underline{F} = [\,F_x \;\; F_y\,]^{\mathrm{T}}$ consists of the Cartesian (xy) forces applied at the end-effector. The E matrix maps the active joint torques $\underline{\tau}_m$, to the joint space while E_2 matrix maps the task-space end-effector force $\underline{F}$, to the joint space. Detailed expressions for the resulting matrices H_u, $\underline{V}$ E, and E_2 are given in Appendix A. However, as we will note later, the control scheme will be developed using the dynamics EOM of an unconstrained system. Hence, we obtain the reduced feasible-space (unconstrained) dynamics by projecting these extended-space constrained dynamic EOM into the feasible motion space. This is realized by premultiplying these EOM by S^T as

$$S^T H_u\ddot{\underline{q}} + S^T\underline{V} = S^T E\underline{\tau}_m + S^T E_2\underline{F} - S^T A^T\underline{\lambda}. \tag{9}$$

Within the extended configuration space of the articulated structure, the orthogonality of the null-space matrix to the constraint matrix ($S^T A^T = 0$) helps eliminate the Lagrange multipliers. By substituting $\ddot{\underline{q}} = S\ddot{\underline{z}} + \dot{S}\dot{\underline{z}}$ into Eq. (9), the constraint-free reduced form[6,20] may be written as

$$H\ddot{\underline{z}} + C\dot{\underline{z}} + \underline{g} = \underline{\tau} + \underline{\tau}_E \tag{10}$$

where $H = S^T H_u S$ is the $n \times n$ symmetric positive-definite inertia matrix, $C = S^T H_u\dot{S}$, $\underline{g} = S^T\underline{V}$, and $\underline{\tau} = S^T E\underline{\tau}_m$ is an $n \times 1$ vector of independent generalized actuation forces, and $\tau_E = S^T E_2\underline{F}$ is an $n \times 1$ vector of independent generalized forces due to external forces acting on the manipulator.

4. Decoupled Task- and Null-Space Dynamic Control Strategy

The focus of this paper is the development of a dynamic-level control routine for the WMM that allows for independent dynamic control of both the task-space (external end-effector) and the null-space (internal manipulator DOF). The primary task is assumed to be one of controlling the motion and/or force interactions of the end-effector with

https://doi.org/10.1017/S0263574706003328 Published online by Cambridge University Press

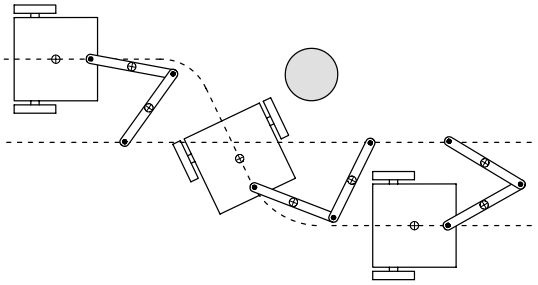


Fig. 4. WMM with alternate specification of desired end-effector and base trajectories.

the attached payload/external environment. Once the primary end-effector task has been accomplished, the secondary task is assumed to be one of controlling the surplus DOF within the system (such as the relative pose of the mobile robot base and arms). In this work, we use the extra configuration redundancy to our advantage by controlling mid-axle point of the differentially driven wheels to follow another specified trajectory, as depicted in Fig. 4.

We adapt a technique developed for control of redundant serial-chain robots[21] for use with our nonholonomic WMM. This nonlinear control method separates the equations of motion into the external and internal dynamics and allows the two to be controlled independently. The external dynamics govern the task-space motion and the internal dynamics govern the null-space motions. In terms of advantages, it allows prioritization and guarantees prioritized tracking control of the task-space desired trajectories in the event of a conflict between the task-space and null-space. An additional advantage is the simplicity of implementation—the difficulty of developing this method mathematically does not increase dramatically as the size of the system increases, as it does with nonlinear feedback linearization techniques. We will present a brief overview here—see ref. [22] for details.

In Eq. (7), the task-space velocities are defined by the vector $\underline{\dot{x}}$ of size p, and the independent joint-space velocities by $\underline{\dot{z}}$ of size n. For a kinematically redundant system, $n > p$, the general solution for the independent joint rates may be written as

$$\underline{\dot{z}} = J^{\#}\underline{\dot{x}} + N\underline{\dot{z}} \tag{11}$$

where $J^{\#}$ is the pseudoinverse of the $p \times n$ Jacobian matrix J and N is the $n \times n$ null-space of J defined as $N = I - J^{\#}J$. This relation is often used for resolved velocity control of kinematically redundant manipulators, and permits prioritized inclusion of various redundancy resolution schemes by way of the null-space. Alternatively, a resolved acceleration control scheme for kinematically redundant manipulators may be written as

$$\underline{\ddot{z}} = J^{\#}(\underline{\ddot{x}} - \dot{J}\underline{\dot{z}}) + N\underline{\ddot{z}}. \tag{12}$$

A weighted pseudoinverse (by the inverse of the manipulator inertia matrix H^{-1}) may also be defined as

$$\bar{J} = H^{-1}J^T(JH^{-1}J^T)^{-1} \tag{13}$$

and the corresponding null-space as $\bar{N} = I - \bar{J}J$. Such a mass-matrix weighted pseudoinverse has geometric significance since as it arises it endows the final task space with a kinetic-energy metric originally defined on the tangent space of a selected manipulator.[23] Hence, we will use the dynamically consistent pseudoinverse for the rest of this work. Further, it is easy to see that this so-called dynamically consistent pseudoinverse reduces to the better-known Moore–Penrose pseudoinverse when $H^{-1} = I$. As noted in the literature, the use of this dynamically consistent pseudoinverse $\bar{J}$ and $\bar{N}$ simplifies the process of decoupling the task-space and null-space dynamics. Premultiplying both sides of Eq. (10) by $I = J^T\bar{J}^T + \bar{N}^T$ and simplifying yields

$$J^T\underline{F} + \bar{N}^T\underline{\tau} = \text{term}_1 + \text{term}_2 + \text{term}_3 \tag{14}$$

where

$$\begin{aligned}
\text{term}_1 &= J^T\bar{J}^T(H\bar{J}(\underline{\ddot{x}} - \dot{J}\underline{\dot{z}}) + C\underline{\dot{z}} + \underline{g} - \underline{\tau}_E)\\
\text{term}_2 &= \bar{N}^T(H\bar{N}\underline{\ddot{z}} + C\underline{\dot{z}} + \underline{g} - \underline{\tau}_E)\\
\text{term}_3 &= J^T\bar{J}^TH\bar{N}\underline{\ddot{z}} + \bar{N}^TH\bar{J}(\underline{\ddot{x}} - \dot{J}\underline{\dot{z}})
\end{aligned}$$

The right-hand side of this equation is composed of three terms: term_1 filters the overall dynamics using $J^T\bar{J}^T$ to allow only the task-space dynamics to pass through. Likewise, term_2 uses $\bar{N}^T = I - J^T\bar{J}^T$ to retain the null-space component of the combined dynamics. term_3 includes all the cross-coupling dynamic terms and become identically zero when the dynamically consistent pseudoinverse is employed. Thus, the final EOM may be expressed in the task space as

$$W(\underline{z})\underline{\ddot{x}} + \underline{\mu}(\underline{z}, \underline{\dot{z}}) + \underline{\gamma}(\underline{z}) = \underline{F} + \underline{F}_E \tag{15}$$

where $W = \bar{J}^TH\bar{J} = (JH^{-1}J^T)^{-1}$ is the $p \times p$ symmetric positive-definite mass matrix, $\underline{\mu} = \bar{J}^TC\underline{\dot{z}} - W\dot{J}\underline{\dot{z}}$ and $\underline{\gamma} = \bar{J}^T\underline{g}$ are the $p \times 1$ vectors that include Coriolis, centrifugal and gravitational forces, $\underline{F} = \bar{J}^T\underline{\tau}$ is the $p \times 1$ vector of actuation forces, and $\underline{F}_E = \bar{J}^T\underline{\tau}_E$ is the $p \times 1$ vector of external manipulator forces (all expressed in task-space coordinates). The control input that successfully decouples the task space and configuration space can then be defined as

$$\underline{\tau} = J^TW(\underline{u} - \dot{J}\underline{\dot{z}}) + \bar{N}^TH(\underline{v} + \dot{\bar{J}}\underline{\dot{x}}) + C\underline{\dot{z}} + \underline{g} + J^T\underline{F}_E \tag{16}$$

where $\underline{u}$ and $\underline{v}$ are the control laws for the task-space and configuration-space, respectively. Since we use a dynamically consistent pseudoinverse to partition the controller, the task-space and configuration-space controllers are fully decoupled. We also note that the null-space controller input is filtered through the dynamically consistent null-space matrix, thus contributing only those torques that do not affect the task-space behavior. Such a prioritized and decoupled controller can now be used as a redundancy resolution scheme to control these redundant WMMs. After substituting Eq. (16) into Eq. (14) and simplifying, the

https://doi.org/10.1017/S0263574706003328 Published online by Cambridge University Press

final equivalent-controlled closed loop dynamics in the independent task space may be written as

$$\underline{u} - \ddot{\underline{x}} = 0. \tag{17}$$

Hence for the task-space, we impose the structure of a task-space impedance controller[24]

$$\underline{u} = \ddot{\underline{x}}_d + k_v \dot{\underline{e}} + k_p \underline{e} + k_f(\underline{F}_d - \underline{F}_E) \tag{18}$$

where $\ddot{\underline{x}}_d$ is the desired acceleration; $\underline{e} = \underline{x}_d - \underline{x}$ is the position error; $\dot{\underline{e}} = \dot{\underline{x}}_d - \dot{\underline{x}}$ is the velocity error; k_v, k_p, and k_f are constants; and $\underline{F}_d$ is the desired end-effector force which creates the closed-loop task-space behavior of a second-order spring-damper-mass with a driving force determined by the desired impedance as:

$$\ddot{\underline{e}} + k_v \dot{\underline{e}} + k_p \underline{e} = -k_f(\underline{F}_d - \underline{F}_E) \tag{19}$$

where $\ddot{\underline{e}} = \ddot{\underline{x}}_d - \ddot{\underline{x}}$. The selection of the gains k_f, k_v, and k_p can now be done by appropriate linear pole-placement techniques.

Equation (16) guarantees that any resultant task-space dynamics are independent of the null-space dynamics. The control inputs that govern the null-space motions are the same torques of the two wheels and the two arm motors. The basic approach remains one of determining a closed-loop control vector $\underline{v} = [v_R v_L v_1 v_2]^{\mathrm{T}}$ as a function of the states of the system to permit a regulation of a meaningful desired output quantity. However, any resulting torques are filtered through the null-space operator $\bar{N}^T H$ so as to ensure consistency with underlying task-space motions. However, it is also worth noting that physical actuators with restrictions on peak output capability can sometimes create limitations on the range of selected values.

There are several possibilities for a meaningful set of output quantities. For example, we could choose to control the orientations of the base and two manipulator arms to fully specify the extended posture. However, we chose the *xy*-coordinates midpoint of the axle of the WMM base as the output. Controlling two such null-space outputs, in addition to two task-space outputs, effectively eliminates all redundancy within the system. Similarly, while one has the freedom to use any number of control routines for this purpose, we choose to use a proven kinematic tracking control method.[25, 26] The principal attractiveness lies in being able to the graceful extend the "posture tracking" controller to achieve "posture stabilization" of the WMR base coupled with the simplicity of implementation as an online motion-planner/controller.

Given the state of a reference virtual unicycle robot as $\underline{z}_r(t) = (x_r(t), y_r(t), \phi_r(t))$, actual robot state $\underline{z}(t) = (x(t), y(t), \phi(t))$, and a reference $(v_r(t), \omega_r(t))$, the goal is to determine a set of feedback controls $\begin{pmatrix} v_s \\ w_s \end{pmatrix} = \underline{f}(\underline{z}, \underline{z}_r, v_r, \omega_r)$ such that $\lim_{t\to\infty}[\underline{z}(t) - \underline{z}_r(t)] = 0$. The system is driven to reduce the error between the reference robot and the actual robot, $\underline{e} = [e_1 e_2 e_3]^{\mathrm{T}}$, expressed in moving frame coordinates as

$$\begin{bmatrix} e_1 \\ e_2 \\ e_3 \end{bmatrix} = \begin{bmatrix} \cos\phi & \sin\phi & 0 \\ -\sin\phi & \cos\phi & 0 \\ 0 & 0 & 1 \end{bmatrix} \begin{bmatrix} x_r - x \\ y_r - y \\ \phi_r - \phi \end{bmatrix}. \tag{20}$$

The final nonlinear control set points for the forward and angular velocities may be written as

$$\begin{bmatrix} v_s \\ \omega_s \end{bmatrix} = \begin{bmatrix} v_r \cos e_3 + k_1(v_r, \omega_r) e_1 \\ \omega_r + k_2(v_r, \omega_r) v_r \dfrac{\sin(e_3)}{e_3} e_2 + k_1(v_r, \omega_r) e_3 \end{bmatrix} \tag{21}$$

with constant gains ξ and $b > 0$ and coefficients $k_1(\omega_r, v_r) = 2\xi\sqrt{(\omega_r^2 + b v_r^2)}$ and $k_2 = b$ can now be guaranteed to asymptotically track any continuously moving trajectory (i.e., $v_r \neq 0$ and $\omega_r \neq 0$ simultaneously, which would be the case for a point-stabilization problem). Hence, in the extension to point stabilization, the reference linear velocity used in Eq. (21) can be modified as

$$v_r = v_{rd} - k_5\sqrt{(x_r - x)^2 + (y_r - y)^2} + k_6\|\underline{e}\|^2 \sin(t)$$
$$\|\underline{e}\| = \sqrt{e_1^2 + e_2^2 + e_3^2} \tag{22}$$

where k_5 and k_6 are constant gains and v_{rd} is the nominal desired linear reference velocity. By preventing both reference robot velocities, v_r and ω_r, from becoming zero simultaneously while a pose-error exists, this allows a direct use of the original nonlinear feedback law for the posture-stabilization problem. An interested reader is referred to refs. [25] and [26] or Chapter 7 in Canudas de Witt *et al.*[9] for detailed discussion.

For a kinematically controlled mobile base, these desired wheel velocities would then have to be input into another control loop to ensure the desired wheel velocities were attained. In our torque-controlled system, this is explicitly implemented as a torque proportional to the error in achieving desired wheel-rates as

$$\begin{bmatrix} v_R \\ v_L \end{bmatrix} = \begin{bmatrix} \frac{r}{2} & \frac{r}{2b} \\ \frac{r}{2} & \frac{-r}{2b} \end{bmatrix} \begin{bmatrix} k_{pv}(v_s - v) \\ k_{p\omega}(\omega_s - \omega) \end{bmatrix}, \quad \begin{bmatrix} v_1 \\ v_2 \end{bmatrix} = \begin{bmatrix} 0 \\ 0 \end{bmatrix}. \tag{23}$$

Suitable gains were selected for the base motion to provide a stable/damped convergence with minimal oscillation in both the linear and rotational velocities while the arm-control inputs are set to zero.

5. Simulation Results

We developed a MATLAB/Simulink model (see Fig. 5) of the mobile-manipulator dynamics and performed extensive tests in order to verify the decoupled dynamic control strategies. The WMM was required to track a variety of task-space and null-space motion/force tasks varying from tracking

https://doi.org/10.1017/S0263574706003328 Published online by Cambridge University Press

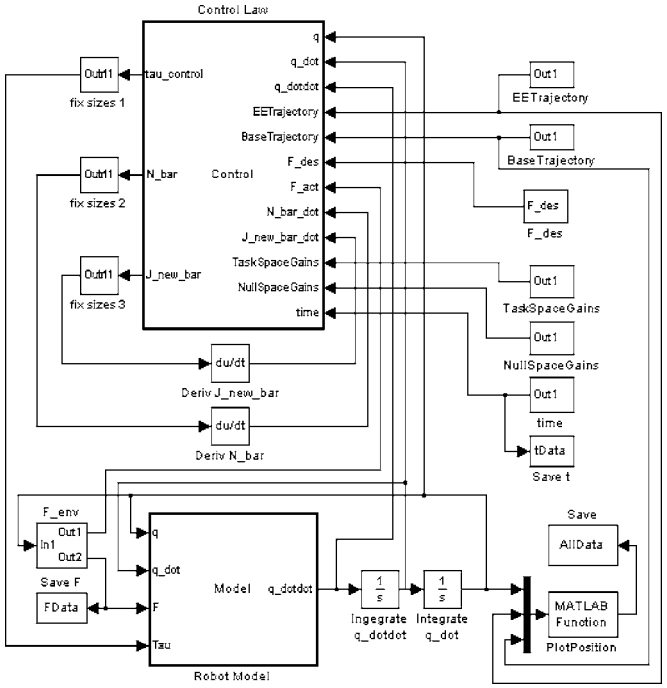


Fig. 5. Simulink block diagram of simulation routine.

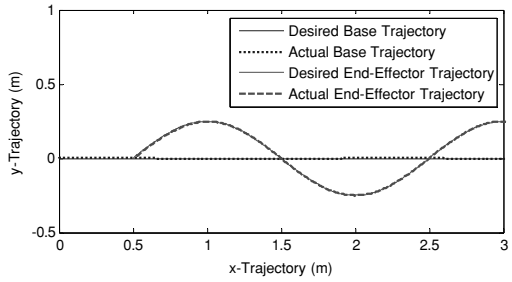


Fig. 6. End-effector tracks a sinusoidal wave and base tracks a straight line.

complex sinusoidal and square-wave paths to stabilization to a constant value. Conflicting task-space and null-space tasks were also considered to verify the preferential satisfaction of the task-space requirements.

In the results to follow, the motion-trajectories presented are those of the end-effector of the WMM and mid-axle point of mobile base moving in the horizontal Cartesian plane. The solid red and blue lines represent the desired end-effector and mobile base trajectories, while the dotted red and blue lines represent the corresponding actual end-effector and mobile base trajectories, respectively. The selected value of control gains are shown in Table 3.

Figure 6 shows the result when the end-effector is prescribed a sinusoidal trajectory with $y(t) = 0.25\sin(\pi t)$ m and mobile base is required to track a straight line trajectory with a desired linear velocity along each straight-line segment of 0.125 m/s. In the results, we see that the actual trajectories (of both end-effector and base) are almost superposed on the desired-trajectories and such good tracking performance is to be expected when the desired trajectories lie within system capabilities.

Additionally, we created desired trajectories for the mobile base and the end-effector that would pose challenges so as to illustrate the prioritized and preferential satisfaction of the end-effector trajectory over that of the base. Both the end-effector and mobile base are now required to track square-wave trajectories (sequences of straight lines and sharp corners) with a desired linear velocity of 0.125 m/s along each straight-line segment.

Figure 7 shows the results wherein the actual end-effector closely tracks the desired trajectory while the mobile base is unable to do so. Such prioritized tracking performance by the end-effector trajectory (at the cost of mobile base

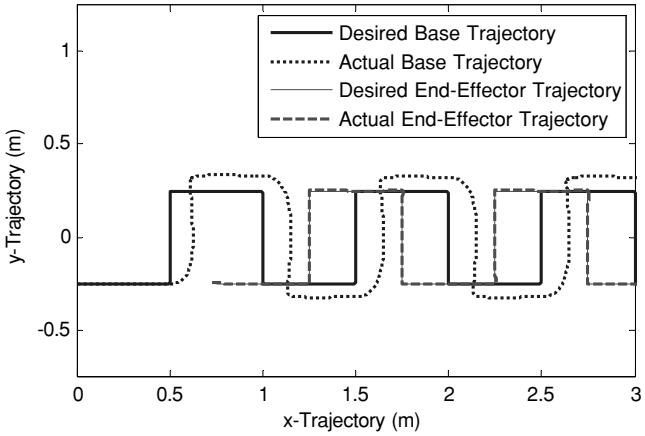


Fig. 7. End-effector and base track square wave.

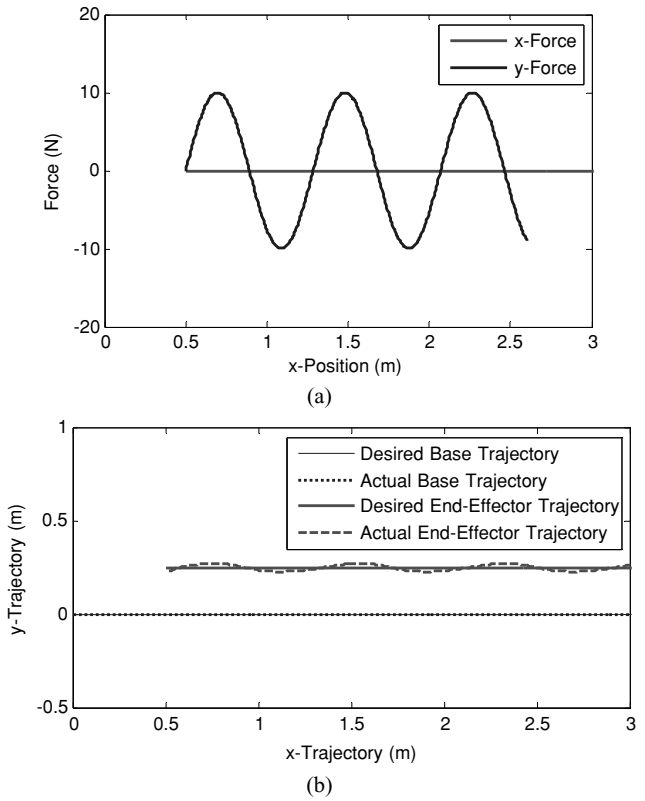


Fig. 8. (a) Sinusoidal disturbance force $F_y = 10\sin(4x)$ N applied to end-effector. (b) Resulting end-effector trajectory.

https://doi.org/10.1017/S0263574706003328 Published online by Cambridge University Press

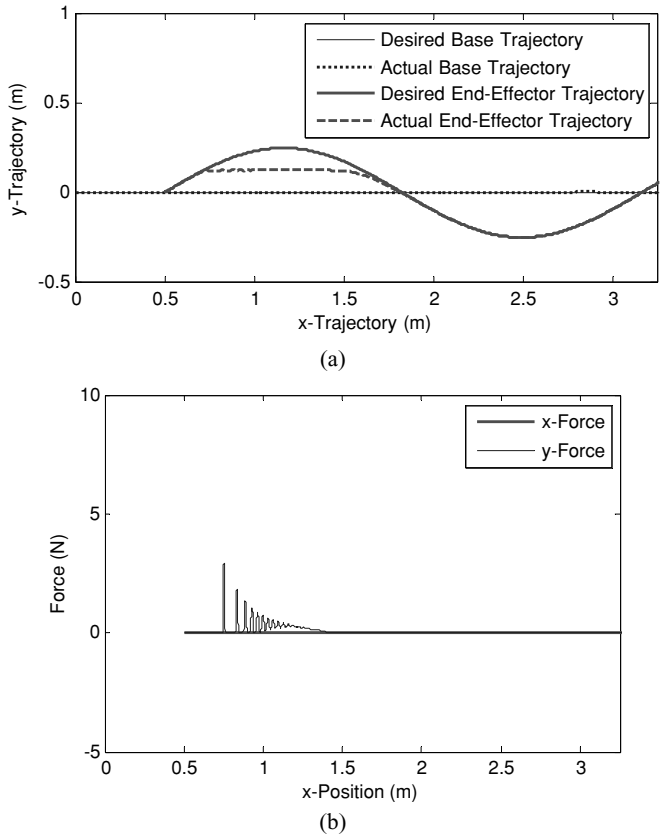


Fig. 9. (a) Tracking performance with desired end-effector trajectory $y_{EE} = 0.25\sin(x_{EE})$ m and desired force $F_y = 0$ N upon encountering a wall at $y = 0.125$ m. (b) Resulting interaction force transients are quickly damped out.

performance) occurs very naturally when the challenging requirements are introduced.

In the third test, the desired end-effector trajectory is a line $x_{EE}(t) = t$m, $y_{EE}(t) = 0.25$ m, while the desired mobile base trajectory is the line $x_M = t$m, $y_M(t) = 0$ m. An unmeasured sinusoidal force disturbance $F_x = 0$ N, $F_y = 10\sin(4x)$ N shown in Fig. 8(a) is imposed on the end-effector to study tracking performance. This significant force disturbance is damped out under the influence of the hybrid-impedance controller resulting in the small end-effector trajectory disturbance error seen in Fig. 8(b).

For the fourth test, the desired base trajectory is the line $x_M = t$m, $y_M(t) = 0$ m while the desired end-effector trajectory is $y_{EE} = 0.25\sin(x_{EE})$ m. An environment constraint (wall) is created at $y = 0.125$ m and modeled as a compliance with a spring constant of $k = 1000$ N/m. The desired end-effector/wall interaction force is set to $F_y = 0$ N. In Fig. 9(a), we see that the end-effector follows the desired trajectory closely as long its does not conflict with the environment constraint. When $y_{EE} > 0.125$ m the end-effector is forced to follow a trajectory defined by the environment constraint and resumes good tracking of the desired end-effector postion once $y_{EE} < 0.125$ m. Figure 9(b) shows the resulting interaction force profile, which is quickly damped out after the initial impact.

6. Discussion and Continuing Work

The nonholonomic base and the significant inherent redundancy create challenges for control of end-effector motion/force outputs in task space. However, realizing decentralized large-payload manipulation operations by a fleet of nonholonomic WMMs requires each manipulator to dynamically control its end-effector motions/forces. Thence, the focus of this paper was the dynamic modeling and subsequent development of a dynamic-level redundancy-resolution strategy for the nonholonomic WMM. The primary task was assumed to be one of controlling the motion and/or force interactions of the end-effector with respect to the attached payload/external environment. Once the primary end-effector task has been accomplished, the secondary task is assumed to be one of controlling the surplus DOF within the system (relative pose of the mobile base).

The results illustrate the capabilities for simultaneously controlling both the motion and interaction force behavior of the nonholonomic WMM. Furthermore, by virtue of the nonlinear feedback linearization, any desired behavior (specified in terms of damping ratio, natural frequency, and time constant) may be prescribed and realized for end-effector. The results also demonstrate the ability to simultaneously follow complex end-effector and mobile base trajectories with a natural preference given to end-effector tracking performance. A physical prototype, seen in Fig. 10, is currently being designed and constructed for experimental validation of these results.

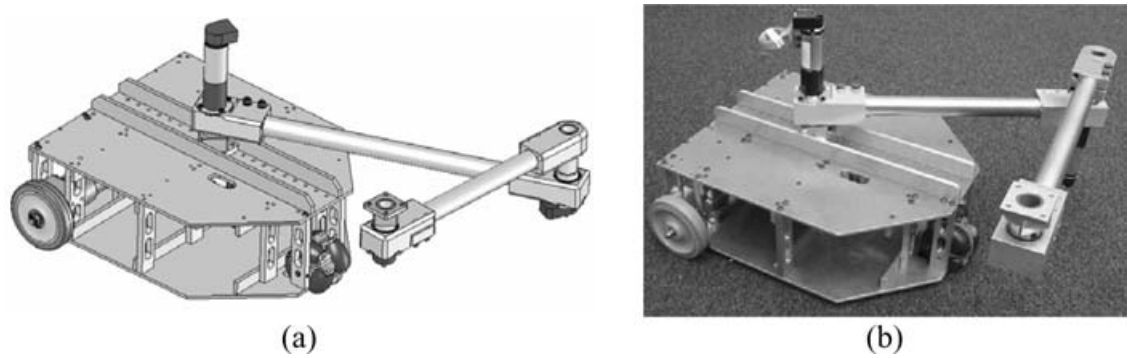


Fig. 10. Individual mobile robot. (a) CAD model. (b) Physical prototype.

https://doi.org/10.1017/S0263574706003328 Published online by Cambridge University Press

Acknowledgment

We gratefully acknowledge the support from National Science Foundation CAREER Award (IIS-0347653) for this research effort.

References

1. C. P. Tang and V. Krovi, "Manipulability-Based Configuration Evaluation of Cooperative Payload Transport by Mobile Robot Collectives," *Proceedings of the 2004 ASME Design Engineering Technical Conferences and Computers and Information in Engineering Conference* (2004).
2. M. Abou-Samah and V. Krovi, "Optimal Configuration Selection for a Cooperating System of Mobile Manipulators," *Proceedings of the 2002 ASME Design Engineering Technical Conference* (2002).
3. H. Seraji, "A unified approach to motion control of mobile manipulators," *Int. J. Robot. Res.* **17**(2), 107–118 (1998).
4. Y. Yamamoto, Control and Coordination of Locomotion and Manipulation of a Wheeled Mobile Manipulator *Ph.D. Thesis* (Philadelphia, PA: University of Pennsylvania, 1994).
5. Y. Yamamoto and X. Yun, "Coordinating locomotion and manipulation of a mobile manipulator," *IEEE Trans. Autom. Control* **39**(6), 1326–1332 (1994).
6. R. Colbaugh, M. Trabatti and K. Glass, "Redundant nonholonomic mechanical systems: characterization and control," *Robotica* **17**(2), 203–217 (1999).
7. R. W. Brockett, "Control Theory and Singular Riemannian Geometry," **In**: *New Directions in Applied Mathematics* (P. J. Hilton and G. S. Young eds.) (Springer-Verlag, New York, 1981) pp. 11–27.
8. R. M. Murray and S. S. Sastry, "Nonholonomic motion planning: steering using sinusoids," *IEEE Trans. Autom. Control* **38**(5), 700–716 (1993).
9. C. Canudas deWitt, B. Siciliano and G. Bastin, *Theory of Robot Control* (Springer-Verlag, Berlin, 1996).
10. Z. Li and J. F. Canny, *Nonholonomic Motion Planning* (Kluwer Academic, Boston, MA, 1993).
11. J.-C. Latombe, *Robot Motion Planning* (Kluwer Academic, Boston, MA, 1991).
12. Y. Nakamura, *Advanced Robotics: Redundancy and Optimization* (Addison-Wesley, CA, 1991).
13. D. E. Whitney, "Resolved motion rate control of manipulators and human prostheses," *IEEE Trans. Man-Mach. Syst.* **MMS-10**, 47–53 (1969).
14. V. Kumar and K. J. Waldron, "Force distribution in walking vehicles on uneven terrain," *ASME J. Mechanisms, Transmiss., Autom. Design* **112**(1), 90–99 (1990).
15. J. Kerr and B. Roth, "Analysis of multifingered hands," *Int. J. Robotics Res.* **4**(4), 3–17 (1986).
16. X. Yun and V. Kumar, "An approach to simultaneous control of trajectory and interaction forces in dual arm configurations," *IEEE Trans. Robot. Autom.* **7**(5), 618–625 (1991).
17. O. Khatib, "A unified approach to motion and force control of robot manipulators: the operational space formulation," *IEEE J. Robot. Autom.* **RA-3**(1), 43–53 (1987).
18. O. Khatib, K. Yokoi, K. Chang, D. Ruspini, R. Holmberg and A. Casal, "Vehicle/Arm Coordination and Multiple Mobile Manipulator Decentralized Cooperation," *Proceedings of the1996 IEEE/RSJ International Conference on Intelligent Robots and Systems* (1996) pp. 546–553.
19. J. Tan, N. Xi and Y. Wang, "Integrated task planning and control for mobile manipulators," *Int. J. Robot. Res.* **22**(5), 337–354 (2003).
20. N. Sarkar, Y. Xiaoping and K. Vijay, "Control of mechanical systems with rolling constraints: application to dynamic control of mobile robots," *Int. J. Robot. Res.* **13**(1), 55–69 (1994).
21. B. Nemec and L. Zlajpah, "Null space velocity control with dynamically consistent pseudo-inverse," *Robotica* **18**(5), 513–518 (2000).
22. G. White, Simultaneous motion and interaction force control of a nonholonomic mobile manipulator *M.S. Thesis* (Dept. Mechanical & Aerospace Engineering, State University of New York at Buffalo, NY, 2006).
23. R. Murray, Z. Li and S. Sastry, *A Mathematical Introduction to Robotic Manipulation* (CRC Press LLC, Boca Raton, Florida, 1993).
24. R. Anderson and M. Spong, "Hybrid impedance control of robotic manipulation,"*IEEE J. Robot. Autom.* **4**(5), 549–556 (1988).
25. C. Samson and K. Ait-Abderrahim, "Feedback Stabilization of a Nonholonomic Wheeled Mobile Robot," *Proceedings of the 1991 IEEE/RSJ International Workshop on Intelligent Robots and Systems* (1991) pp. 1242–1247.
26. C. Samson and K. Ait-Abderrahim, "Feedback Control of a Nonholonomic Wheeled Cart in Cartesian Space," *Proceedings of the 1991 IEEE International Conference on Robotics and Automation* (1991) pp. 1136–1141.

Appendix A

$$H_u = \begin{bmatrix} p_1 & 0 & -p_2\sin(\phi) & 0 & 0 & -p_3\sin(\theta_1) & -p_4\sin(\theta_2) \\ 0 & p_1 & p_2\cos(\phi) & 0 & 0 & p_3\cos(\theta_1) & p_4\cos(\theta_2) \\ -p_2\sin(\phi) & p_2\cos(\phi) & p_5 & 0 & 0 & p_8 & p_9 \\ 0 & 0 & 0 & p_7 & 0 & 0 & 0 \\ 0 & 0 & 0 & 0 & p_7 & 0 & 0 \\ -p_3\sin(\theta_1) & p_3\cos(\theta_1) & p_8 & 0 & 0 & p_6 & p_{11} \\ -p_4\sin(\theta_2) & p_4\cos(\theta_2) & p_9 & 0 & 0 & p_{11} & p_{10} \end{bmatrix}$$

where

$$p_1 = m_c + m_1 + m_2$$
$$p_2 = L_a(m_1 + m_2)$$
$$p_3 = m_1 L_{cm1} + m_2 L_1$$
$$p_4 = m_2 L_{cm2}$$
$$p_5 = L_a^2(m_1 + m_2) + I_c$$
$$p_6 = m_1 L_{cm1}^2 + m_2 L_1^2 + I_1$$
$$p_7 = m_w r^2 + I_w$$
$$p_8 = L_a(m_1 L_{cm1} + m_2 L_1)\cos(-\phi + \theta_1)$$
$$p_9 = m_2 L_a L_{cm2}\cos(-\phi + \theta_2)$$
$$p_{10} = m_2 L_{cm2}^2 + I_2$$
$$p_{11} = m_2 L_1 L_{cm2}\cos(\theta_1 - \theta_2)$$

$$\underline{V} = [V_1 \quad V_2 \quad V_3 \quad c_R\dot{\theta}_R \quad c_L\dot{\theta}_L \quad V_6 \quad V_7 \quad]^T,$$

where

$$V_1 = -L_a(m_1 + m_2)\cos(\phi)\dot{\phi}^2 - (m_1 L_{cm1} + m_2 L_1)\theta_1^2\cos(\theta_1) - m_2 L_{cm2}\cos(\theta_2)\theta_2^2$$

$$V_2 = -L_a(m_1 + m_2)\sin(\phi)\dot{\phi}^2 - (m_1 L_{cm1} + m_2 L_1)\theta_1^2\sin(\theta_1) - m_2 L_{cm2}\sin(\theta_2)\theta_2^2$$

$$V_3 = -(m_1 L_{cm1} + m_2 L_1)L_a\dot{\theta}_1^2\sin(-\phi + \theta_1) - m_2 L_a L_{cm2}\dot{\theta}_2^2\sin(-\phi + \theta_2) - c_1\dot{\theta}_1 + c_1\dot{\phi}$$

$$V_6 = (m_1 L_{cm1} + m_2 L_1)L_a\dot{\phi}^2\sin(-\phi + \theta_1) - c_1\dot{\phi} - c_2\dot{\theta}_2 + (c_1 + c_2)\dot{\theta}_1 + m_2 L_1 L_{cm2}\dot{\theta}_2^2\sin(\theta_1 - \theta_2)$$

$$V_7 = m_2 L_{cm2} L_a\dot{\phi}^2\sin(-\phi + \theta_2) - m_2 L_{cm2} L_1\dot{\theta}_1^2\sin(\theta_1 - \theta_2) + c_2\dot{\theta}_2 - c_2\dot{\theta}_1$$

https://doi.org/10.1017/S0263574706003328 Published online by Cambridge University Press

$$E = \begin{bmatrix} 0 & 0 & 0 & 0 \\ 0 & 0 & 0 & 0 \\ 0 & 0 & -1 & 0 \\ 1 & 0 & 0 & 0 \\ 0 & 1 & 0 & 0 \\ 0 & 0 & 1 & -1 \\ 0 & 0 & 0 & 1 \end{bmatrix}, \quad E_2 = \begin{bmatrix} 1 & 0 \\ 0 & 1 \\ -L_a \sin(\phi) & L_a \cos(\phi) \\ 0 & 0 \\ 0 & 0 \\ -L_1 \sin(\theta_1) & L_1 \cos(\theta_1) \\ -L_2 \sin(\theta_2) & L_2 \cos(\theta_2) \end{bmatrix}$$

Appendix B

Table 1. Kinematic parameters of the WMM.

Parameter	Description	Values
b	distance from wheel to WMR center	0.182 m
d	distance from wheel axis to center of mass	0.116 m
r	wheel radius	0.0508 m
L_1	length of link1	0.514 m
L_2	length of link2	0.362 m
L_{cm1}	position of center of mass of link1	0.252 m
L_{cm2}	position of center of mass of link2	0.243 m
(x_c, y_c)	absolute position of the center of mass	
ϕ	absolute rotation angle of WMR	
θ_R, θ_L	wheel angular displacement	
θ_1, θ_2	absolute link angles w.r.t the global frame	

Table 2. Dynamic parameters.

Parameter	Description	Values
I_w	wheel inertia, about the wheel axis/center of mass	2.0×10^{-4} kg m^2
c_L, c_R	wheel damping	0.1 kg m^2/s
m_w	wheel mass	0.159 kg
m_c	base mass	17.25 kg
I_c	base inertia, about the center of mass/z-axis	0.297 kg-m^2
I_1	link1 inertia, about the center of mass/z-axis	0.148 kg m^2
I_2	link2 inertia, about the center of mass/z-axis	0.0228 kg m^2
m_1	link1 mass	2.56 kg
m_2	link2 mass	1.07 kg
c_1, c_2	Joint damping at points P_a and P_1, respectively	0.1 kg m^2/s
τ_R, τ_L	wheel input torque	
τ_1, τ_2	motor torque input at points P_a and P_1, respectively	
F_x, F_y	environment interaction force at the end-effector	

Table 3. Control gains.

Figures	k_v	k_p	k_2	ξ	k_{pv}	k_{pw}	k_5	k_6	k_f
Fig. 6	10	25	5	2	4	8	0	0	10
Fig. 7	40	400	5	2	4	8	0	0	10
Fig. 8	40	400	5	2	4	8	0	0	10
Fig. 9	10	25	5	2	4	8	0	0	10

https://doi.org/10.1017/S0263574706003328 Published online by Cambridge University Press